Technical note

Journal of High School Science

Aerodynamic optimization of a 50-passenger aircraft for Mach 5 flight

Udaymaan S[1]

Submitted: October 31, 2022, Revised: version 1, January 5, 2023
Accepted: January 21, 2023

Abstract

Designing an aircraft to fly at supersonic/hypersonic speeds comes with many challenges. These are mainly attributed to the shockwaves formed at those speeds, which create unique flow conditions. These challenges lead to unique design considerations in the three pillars of aerospace engineering: propulsion, structures, and aerodynamics. This study is a preliminary design study that explores aerodynamic considerations and provides aerodynamic analysis. The objective was to create an optimal aircraft design for a passenger aircraft at Mach 5 cruise speed with 50 passengers. The design study focussed on the aerodynamic impact (lift and drag) of changing the specifications of the wing, where it explored the effects of changing the wingspan, root incidence angle, and root chord length. Using OpenVSP, a parametric aircraft modeling software, multiple wing iterations were created based on the changing variables listed above. VSPaero, a vortex lattice solver, was then employed to evaluate the wings' aerodynamic performance based on the variables listed above. This design study explored the flight performance metrics of the lift-to-drag ratio, skin friction coefficient, wave drag coefficient, induced drag coefficient, and lift coefficient. Using the data gathered from these simulations, this design study established a relationship between the design variables and their effect on the aerodynamic performance metrics listed above. These relationships and models were then utilized to define an optimization problem that yielded the optimal 50-passenger supersonic aircraft that maximized the lift-to-drag ratio at a cruise speed of Mach 5.

Keywords

Aerospace engineering, Hypersonic, Supersonic, Aircraft design, Optimization, Aerodynamics, Wingspan, Lift to drag ratio, Root incidence angle, Root chord length

[1]Corresponding author: Udaymaan Sidhu, Christian Brothers High School, 4315 Martin Luther King Jr Blvd, Sacramento, CA 95820, USA, umsidhu@gmail.com

Introduction

Aerodynamic challenges of supersonic/ hypersonic flight

Common aerodynamic challenges of supersonic or hypersonic flight arise from the various forms of drag acting on the aircraft and their relation to the lift produced by the aircraft.

One of the most important ways of measuring the aerodynamic performance of an aircraft based on lift and drag is the Lift-to-Drag ratio. The L/D compares the total lift of the aircraft to the total drag of the aircraft. The L/D is calculated by taking the lift coefficient and dividing it by the drag coefficient, $\frac{L}{D}=\frac{C_L}{C_D}$. When all other factors (such as aircraft weight and engine performance) are held constant, the L/D is proportional to the aircraft's range. L/D usually decreases with increasing Mach number. This leads to supersonic/hypersonic aircraft usually having a decreased range compared to modern commercial airliners, such as the Boeing 777x (the Boeing 777x has an L/D of 18 at Mach 0.5, while the BAC Concorde had an L/D of 7.5 at Mach 2) (1). The L/D can be a quick way of determining the aerodynamic efficiency and was a central part of this design study.

Another problem of supersonic flight arises from the different components that make up the total drag. The two that are focused on in this design study were skin friction drag (a component of parasitic drag) and wave drag.

Skin friction drag is a component of parasitic drag, which is drag experienced when a solid object moves through a fluid. Skin friction drag is the result of the viscosity of a fluid flowing over the boundary layer of an object. The magnitude of skin friction drag is the result of the wetted area of an object and the speed at which the fluid is moving over it. The analysis of skin friction drag also has to consider the effect of the laminar flow of the boundary layer transitioning to a turbulent flow, which increases skin friction drag (2, 3). Skin friction drag follows the drag equation, thus it increases with the square of the velocity:

$$D_f=C_{D_f}S_{ref}\frac{\rho V_\infty{}^2}{2}$$

Skin friction drag will have a significant effect on supersonic/hypersonic aircraft, as the velocity of the air flowing over the surface of the aircraft is much higher than that of a trans-sonic operating airliner. While lift also increases with the square of the velocity, hence staying proportional to skin friction drag, the effects of skin friction drag have a multitude of effects on other parameters such as structure. The velocity of supersonic/hypersonic aircraft also greatly affects the transitioning of laminar flow to turbulent flow. The characteristics of flow patterns in a fluid are predicted by Reynolds Number. The Reynolds Number is the ratio of the inertia force to the viscous force of the fluid flowing over an object, and increases with an increase in velocity (4). The Reynolds number is given by: $\Re=\frac{\rho V_\infty L}{\mu}$ A high Reynolds Number predicts a more turbulent flow, and the velocity of supersonic/hypersonic aircraft entails a high Reynolds Number, which results in a substantial drag increase from the turbulent flow. This leads to supersonic and hypersonic aircraft also having to greatly consider a resulting increase in heat transfer (4, 5).

Wave drag at high supersonic to hypersonic speeds is a phenomenon characterized by the formation of shock waves around an aircraft as the result of the Mach number being greater than 1. Wave drag is one of the most important considerations taken into account in designing supersonic and hypersonic aircraft, especially the latter, as wave drag accounts for most of the drag experienced at hypersonic flight. Wave drag accounts for the laminar flow of the boundary layer being separated, usually forming shockwaves formed at the head and the leading edge of the aircraft. This disruption in laminar flow results in a substantial amount of drag at supersonic/hypersonic speeds (6).

Common approaches to overcoming supersonic/ hypersonic speed-related problems

While there is a plethora of research in mitigating supersonic/hypersonic problems in flight from propulsion, structure, and aerodynamics, this design study focussed on aerodynamics; primarily on wing design.

To minimize the skin friction drag, two options were considered. One was to delay the transition to turbulent flow from laminar flow on the wing surface as much as possible (fully laminar flow is practically impossible at supersonic/hypersonic speeds). The second was to accept the inevitability of turbulent flow and adapt designs that incorporate it to reduce skin friction drag (7).

To characterize the wave drag, the most common method used is a version of Paul Whitcomb's "area rule" known as the supersonic area rule. The supersonic area rule expresses wave drag through cross-sectional areas intercepted by Mach planes. The rule demonstrates that low-aspect wing ratios have a wave drag reduction over a wide range of Mach numbers (8). Another method to mitigate wave drag at supersonic/hypersonic speeds is preventing the formation of a detached bow shockwave. Detached bow shockwaves, as opposed to attached oblique shockwaves, are curved and detached from the object they forms on (usually blunt). These shockwaves greatly increases drag at supersonic/hypersonic speeds (9). Supersonic and hypersonic aircraft usually have sharper edges to mitigate bow shocks. Common wing design research in mitigating these issues in supersonic/hypersonic flight can be split into two specific groups: aerofoil design and wing shape.

A common aerofoil design considered in supersonic/hypersonic aircraft is the double wedge aerofoil. Double wedge aerofoils are commonly used in supersonic/hypersonic aircraft. Double wedge aerofoils create Prandtl-Meyer expansion waves as the supersonic flow is turned away from itself on the double wedge geometry. These expansion waves in this expansion region are an infinite amount of weak Mach waves. The supersonic flow over these expansion waves is a mostly smooth (laminar) flow, and the pressure across these expansion waves decreases compared to the high pressure of the supersonic shockwaves on the edges of the aerofoil, creating lift at supersonic/hypersonic speeds (10, 11, 12). The thin leading edge of double wedge aerofoils also has the effect of mitigating the drag caused by detached bow shockwaves, as the thin edge is better at creating an attached oblique shockwave (13).

The delta wing is a common wing design for supersonic/hypersonic aircraft. Delta wings usually classify as low-aspect-ratio wings (where their span to mean-chord ratio is low), where their aspect ratios are usually below 3 in most cases. The Delta wing's low aspect ratio and high sweep angles allow it to stay within the Mach cone, whose angle is determined by the equation below (where θ is in degrees):

$\theta = \sin^{-1}\left(\frac{1}{M}\right)$. Delta wings also provide additional lift at supersonic/hypersonic speeds through vortex lift, a phenomenon created by the suction effect from the geometry of delta wings creating flow separation vortices across their surface (14).

Wing, aerofoil, fuselage, and vertical stabilizer selection

Based on the information above, the parameters of base wing, aerofoil fuselage, and vertical stabilizer were chosen to create the aircraft analyzed in this design study.

The wing chosen was a cropped delta wing (Figure 1). The wing is the only variable that changed within this design study. The base wing's root chord length, sweep, and span was kept the same as the BAC Concorde's wing, since the Concorde was a relatively successful supersonic aircraft. Table 1 shows the base wing's main specifications (components that were changed directly or indirectly for different wing iterations in the study are marked with an asterisk).

Table 1: Base wing specifications

Wing Component	**Value**
Span*	13m
Root Incidence*	0°
Root Chord*	27.66m
Tip Chord	5.6m
Sweep*	76°
Aspect Ratio*	0.71

The chosen aerofoil was a double wedge aerofoil with an almost flat lower half (Figure 2). The aerofoil remained the same across the entire wing. The aerofoil remained constant in each design iteration. Table 2 presents the aerofoil's main specifications. The chosen fuselage was a body based on the Sears-Haack body profile (Figure 3). The Sears-Haack body provided the lowest theoretical amount of wave drag for a given volume and length in supersonic/hypersonic flow (15). The fuselage was based on it for this specific reason. Therefore, the fuselage wave drag was at a low value at all times during each design iteration (the fuselage remained constant). The length of the fuselage was the same as the BAC Concorde. The fuselage was estimated to hold at least fifty people when compared to the fuselage of the BAC Concorde. Table 3 shows the fuselage's main specifications.

Table 2: Aerofoil specifications

Aerofoil Component	**Value**
T/C	0.02
Camber	0.01%
X/C of Max Thickness	0.3

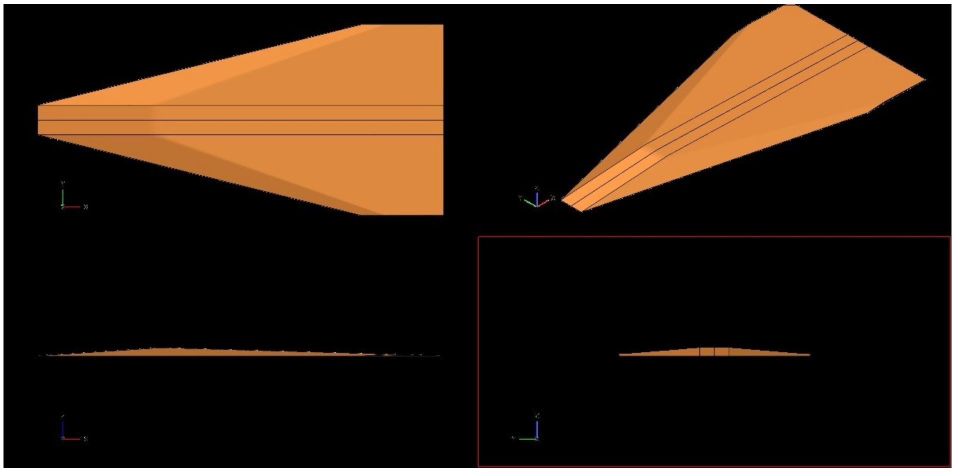

Figure 1: Top, side, front and isometric view of the base wing. The rectangular section in the middle was included to ensure the delta geometry was not cut off when the wing meshed with the fuselage

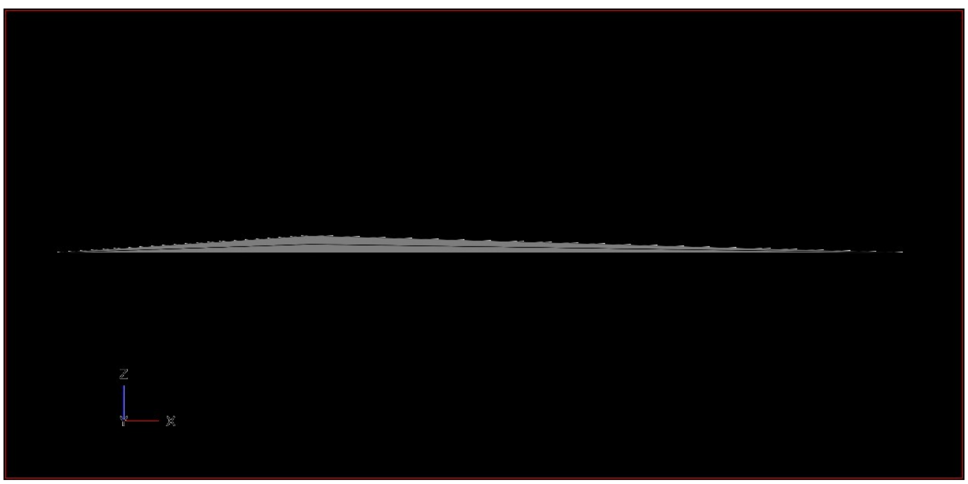

Figure 2: The outline of the aerofoil. This specific one is the root chord aerofoil of the base wing.

Table 3: Fuselage specifications

Fuselage Component	Value
Length	61.66m
Max Width	3m
Fineness Ratio	20.55:1

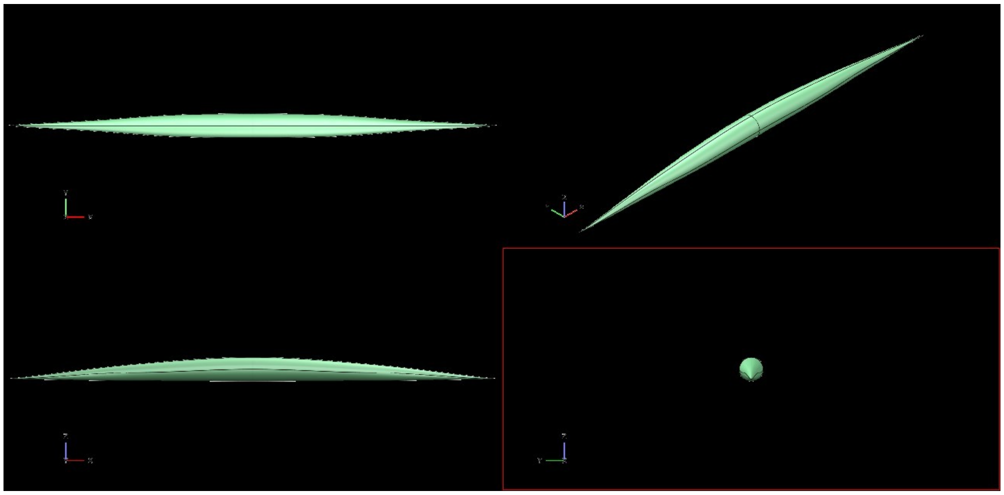

Figure 3: Top, side, front, and isometric view of the fuselage. Even though the fuselage was the same length as the Concorde's fuselage, the width distribution across the fuselage geometry leads it to hold fewer passengers (50) than the Concorde (100).

Table 4: Vertical stabilizer specifications

Vertical Stabilizer Component	**Value**
Length	8.5m
Height	6m
Sweep	50°

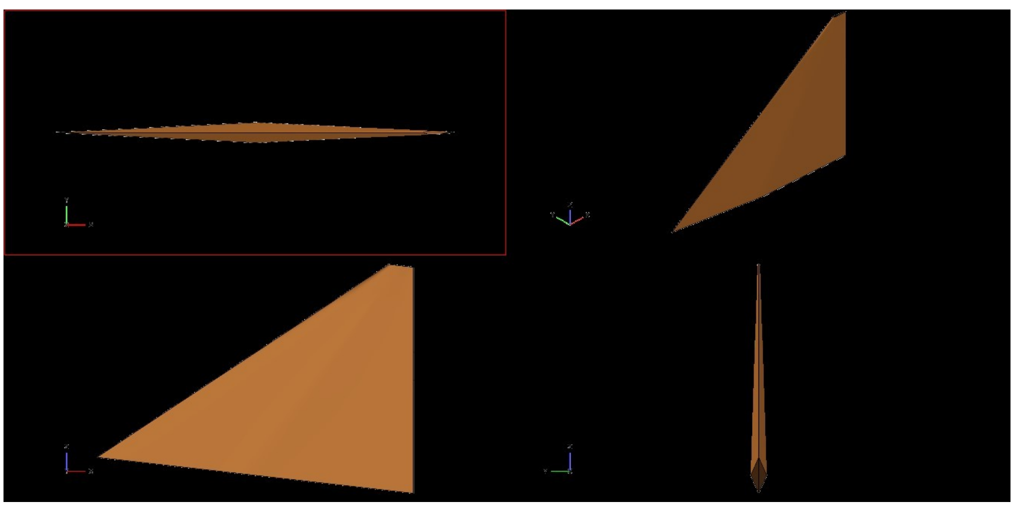

Figure 4: Top, side, front and isometric view of the vertical stabilizer. It is angled upward at the bottom to mesh it properly with the fuselage.

The chosen vertical stabilizer was a simple, double-wedge vertical stabilizer (where the double-wedge aerofoil is symmetrical) (Figure 4). The vertical stabilizer remained constant throughout each design iteration. Table 4 indicates the main specifications of the vertical stabilizer. Each component selected meshed together to create the entire aircraft for each design iteration in OpenVSP (Figure 5).

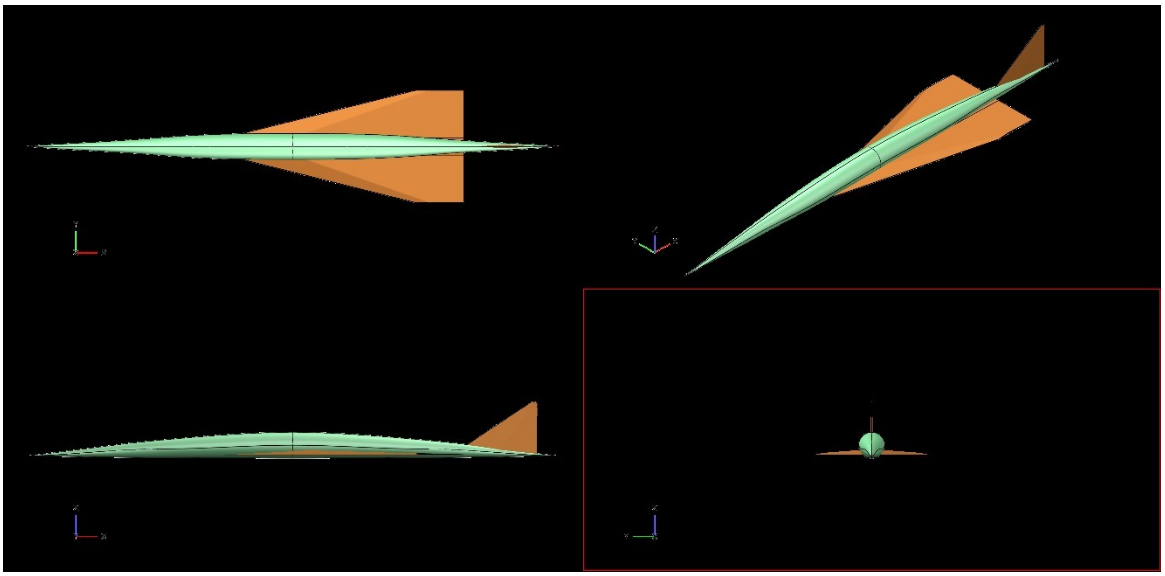

Figure 5: Top, side, front, and isometric view of the entire aircraft for the base aircraft design iteration.

Methods, process and calculation parameters

Some conditions in the software were chosen as fixed values because they were the default and had no effect on the analysis.

VSPaero

To calculate the L/D, lift coefficient, and induced lift coefficient calculation, VSPaero was used.

VSPaero is a fast, vortex lattice solver. Discrete vortices are applied to each panel of a lifting surface based on the degenerate geometry generated in OpenVSP. After setting the preferred parameters, these vortices are then evaluated over the entire surface to obtain the pressure distribution, which can be used to calculate lift and drag forces over the surface (17). These values of lift and drag can then be used to calculate coefficients of drag, coefficient of lift, and the L/D. The wing component of this design study was evaluated using VSPaero to calculate the L/D, coefficient of lift, and coefficient of induced drag.

Due to the fuselage and vertical stabilizer providing almost zero lift, only the wing geometry was used in the solver, as it was the only lifting surface. The wing geometry was chosen by deselecting all other geometries and then selecting the shown geometry (the wing) in the geometry set option of the “Case Setup” tab.

Vortex Lattice Method was selected in this design study for all t hevariables analyzed in VSPaero. In the VSPaero GUI, the VLM geometry was obtained by taking the specified geometry’s degenerate geometry file, which was a simple frame representation of the three-dimensional model. A VLM analysis was chosen by selecting the VLM option in the VSPaero GUI in the “Case Setup” tab.

The estimated center of gravity of the specified geometry of this design study was found using the CG calculation tool in the “Moment Reference Position” tab. Calculating the CG output an estimated CG in the X, Y, and Z directions by showing how far the CG was from the origin of the geometry in each direction.

To ensure a correct interpretation of the wing geometry, the option for obtaining the values of the reference area, mean chord, and projected span of the wing through the actual three-dimensional geometry was chosen in the “Reference Area, Lengths” tab. Although VSPaero’s values are unitless, it was assumed that all geometric measures in the study are in meters.

In the “Flow Condition” tab, the alpha (angle of attack) option was set to one for a value of one degree for every design iteration. The beta (side slip) option was set to zero. The flight velocity in the Mach option was set to 5 for a flight velocity of Mach 5 for all design iterations. The Reynolds number option was given a value based on the Reynolds number obtained through the parasitic drag tool (process for obtaining Reynolds number described in parasitic drag calculations and parameters).

In the wake iterations option in the “Wake” tab, the value was set to 3 iterations to be computed to reduce computation time.

VSPaero runs discrete vortices that are applied to each panel of a lifting surface based on the defined parameters. This gives a pressure distribution across of lifting surface which is used to calculate various factors and coefficients of lift, drag, and aerodynamic performance.

Wave drag tool

To calculate the wave drag coefficient, OpenVSP’s built-in Wave Drag Tool was used.

The wave drag tool built into OpenVSP calculates the wave drag coefficient and cross-sectional area distribution by intersecting the specified geometry by Mach planes across each axis (Mach plane angle determined by user input of Mach number) (18). The entire aircraft model was used to calculate the wave drag coefficient change based on wing design changes.

To ensure that the wing design iterations affected the whole aircraft’s wave drag, the geometry set option in the “Case Setup” tab was set to all geometries (entire aircraft). The amount of Mach plane angle rotations was set to the default of 10, and the number of slices per Mach plane angle rotation was set to the default of 20 in the “Case Setup” tab.

In the “Flow Condition” tab, the free steam velocity was set to a value of 5 for a velocity of Mach 5 to match the set velocity of this design study. To ensure an accurate cross-sectional area analysis from the Mach plane angle slices, the reference area was set to the reference area from the aircraft itself in the "Reference Area" tab.

The wave drag tool uses Mach plane angle slices across the specified geometry to perform its analysis. This gives a cross-sectional area distribution plot and a wave drag coefficient. The angle of the Mach plane is given by the equation, where "θ" is in degrees: $\theta = \sin^{-1}\left(\frac{1}{M}\right)$

Parasitic drag tool

To calculate the skin friction drag Coefficient, OpenVSP's built-in parasitic drag tool was used (only changes in wing root chord and span were analyzed for skin friction drag as root incidence does not affect skin friction due to the parasitic drag tool assuming all geometries are streamlined to the free stream velocity).

The parasitic drag tool built into OpenVSP provides a much more advanced analysis of parasitic drag factors (including overall parasitic drag coefficient and skin friction) over VSPaero's estimated, flat plate skin friction drag coefficient calculation (19). This tool has much more advanced parameters in its process for calculating the parasitic drag, including considering laminar and turbulent flow over a surface, and calculations of the Reynolds number and friction coefficient. It is important to note that this tool assumes that the surface is streamlined to the free stream velocity, and for this reason, changes in the skin friction coefficient were only made on changes to span and root chord length.

In the "Geometry Tab", only the wing geometry was selected for this analysis, and the option for units was set to meters. In the "Equation Selection" tab, two equations for calculating an estimated flat plate average coefficient for friction turbulent or laminar flow needed to be selected. These were used to then calculate the overall estimated laminar friction coefficient based on the percent of laminar flow. The Blasius equation for coefficient of friction under laminar flow was the only one available for laminar flow in the parasitic drag tool, hence it was always selected: $C_f = \frac{1.32824}{\sqrt{\Re}}$

For turbulent flow, various equations could be selected to give an estimated value for the flat plate average coefficient of friction. The equation selected in this design was the Schlichting Compressible equation for coefficient of friction under turbulent flow to address the compressibility of airflow at high supersonic/hypersonic speeds: $C_f = \frac{0.455}{\log()^{2.58}}$

Both equations rely on the Reynolds number of the specified geometry. The Reynolds number was calculated by using the equation: $\Re = \frac{V_\infty L_{ref}}{\mu}$

The reference length of the specified geometry was calculated by the parasitic drag tool using the equation: $L_{ref} = \frac{\bar{c}}{S_{total}}$

In the "Flow Condition" tab, the atmosphere was set to the default U.S. Standard Atmosphere of 1976. After also setting the free stream velocity to Mach 5, and the altitude of 60000 ft (the same altitude that the BAC Concorde, a supersonic airliner, flew at), a set value was input for the flow viscosity at $2.969 \cdot 10^{-7}$ slug/ft^3.

The value for the percent of laminar flow was set to 20%, assuming a semi-laminar and turbulent flow, and the interference factor was set to 1.00. The Form Factor equation selected (there were various Form Factor equations available) for calculating the Form Factor was the default Hoerner Form Factor equation: $FF = 1 + 2\left(\frac{t}{c}\right) + 60\left(\frac{t}{c}\right)^4$

The parasitic drag tool was used to calculate the estimated overall laminar friction coefficient and wetted area for each wing design iteration. These values were then used as part of a manual calculation to find the estimated skin friction coefficient for each wing design iteration. The overall laminar friction coefficient was calculated using the tool by the equation:

$$C_f = C_{f(100\,\%Turb)} - \left(C_{f(\%PartialTurb)} \cdot \%Lam\right) + \left(C_{f(\%PartialLam)} \cdot \%Lam\right)$$

Where:

$C_{f(\%PartialTurb)} = f\left(\mathfrak{R}_{Lam}\right)$, $C_{f(\%PartialLam)} = f\left(\mathfrak{R}_{Lam}\right)$, and $\mathfrak{R}_{Lam} = \mathfrak{R} \cdot \%Lam$

The flat plate drag used to calculate the values above was, in turn, calculated by the parasitic drag tool using the equation: $f = S_{wet} \cdot Q \cdot C_f \cdot FF$ (The friction coefficient in the flat plate drag equation depends on whether the partial turbulent or partial laminar friction coefficient is being calculated, which affects which average flat plate friction coefficient, turbulent or laminar, is being used)

After obtaining the value for the estimated overall laminar friction coefficient, a manual calculation was used to obtain the estimated skin friction coefficient. The equation used was derived from the traditional equation to obtain the skin friction drag coefficient (2):

$$C_{D_f} = \frac{2\,D_f}{\rho V_\infty^2 S_{ref}} = C_f\left(\frac{S_{wet}}{S_{ref}}\right)$$

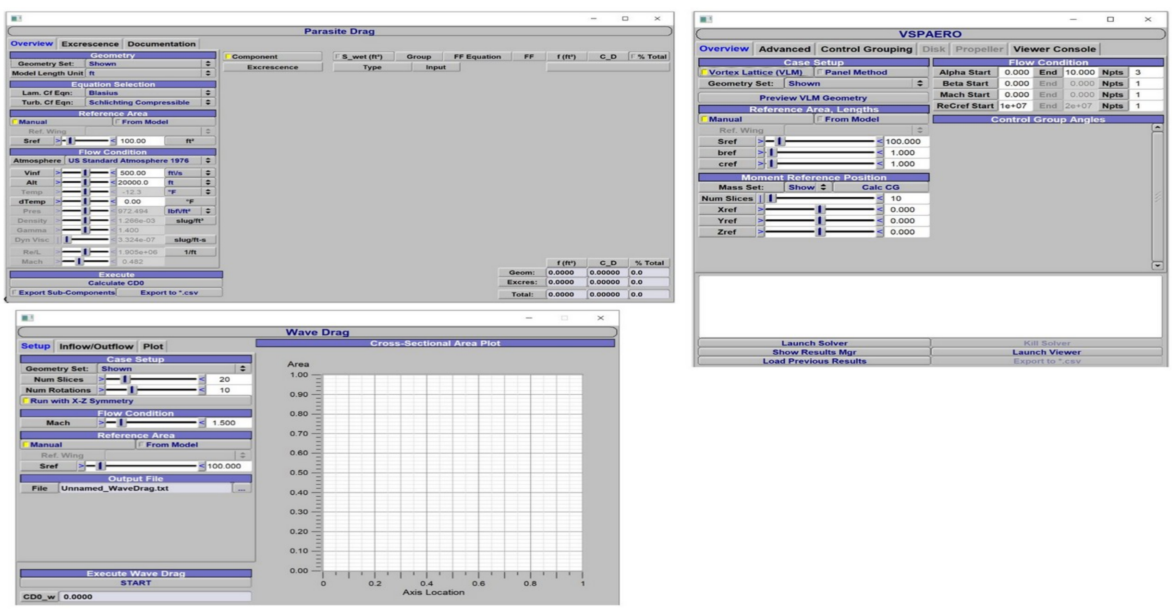

Figure 6: The software GUI (VSPaero, Wave Drag Tool, and Parasitic Drag Tool)

Methods

Using the tools described, the change in the L/D, lift coefficient, induced drag coefficient, wave drag coefficient, and skin friction drag coefficient, based on the change in span, root incidence, and root chord, were calculated. Wing span is the total width of the wing from tip to tip, root incidence is the angle the root chord of the root aerofoil makes with the horizon, and root chord is the length of the root aerofoil from tip to tip.

For the change in span, the base span of 13 m was increased for 5 design iterations (not including the base iteration) in increments of 1 m (base iteration span was 13m and final iteration span was 18 m). These changes were then analyzed for the change in the variables evaluated for this design study.

For the change in root incidence, the base incidence of 0° was increased for 5 design iterations (not including the base iteration) in increments of 1° (base iteration incidence was 0° and final iteration incidence was 5°). These changes were then analyzed for the change in the variables evaluated for this design study.

For the change in root chord, the base chord of 27.66 m was increased for 5 design iterations (not including the base iteration) in increments of 1 m (base iteration chord was 27.66 m and final iteration chord was 32.66 m). These changes were then analyzed for the change in the variables evaluated for this design study.

Results

The effect of design variables on several aerodynamic performance characteristics were evaluated. Figure 7 shows the relationship between the design variables span length, root incidence angle, and root chord length on the aerodynamic properties of induced drag coefficient, wave drag coefficient, and skin friction drag coefficient. Figure 8 shows the relationship between the design variables' span length, root incidence angle, and root chord length on the aerodynamic property of lift coefficient. Figure 9 shows the relationship between the design variables' span length, root incidence angle, and root chord length on the aerodynamic property of L/D.

Changing the span, root incidence, and root chord had a negligible effect on the wave drag coefficient (Figure 7). Increasing the span and the root chord caused a small decrease in the wave drag coefficient, whereas increasing the root incidence caused a small increase. The largest (non significant) change in the wave drag coefficient was caused by increasing the span, decreasing from 0.0012 in the range of 13 m to 15 m to a value of 0.001 in the range of 17 m to 18 m.

Changing the span or the root chord had a negligible effect on the induced drag coefficient (Figure 7), whereas changing the root incidence caused a significant exponential change. The induced wave drag coefficient exponentially increased from 0.00061 at the 0° base, to 0.00663 at 5°.

Figure 7: The relationship between span length, root incidence angle, and root chord length on the aerodynamic properties of induced drag coefficient, wave drag coefficient, and skin friction drag coefficient.

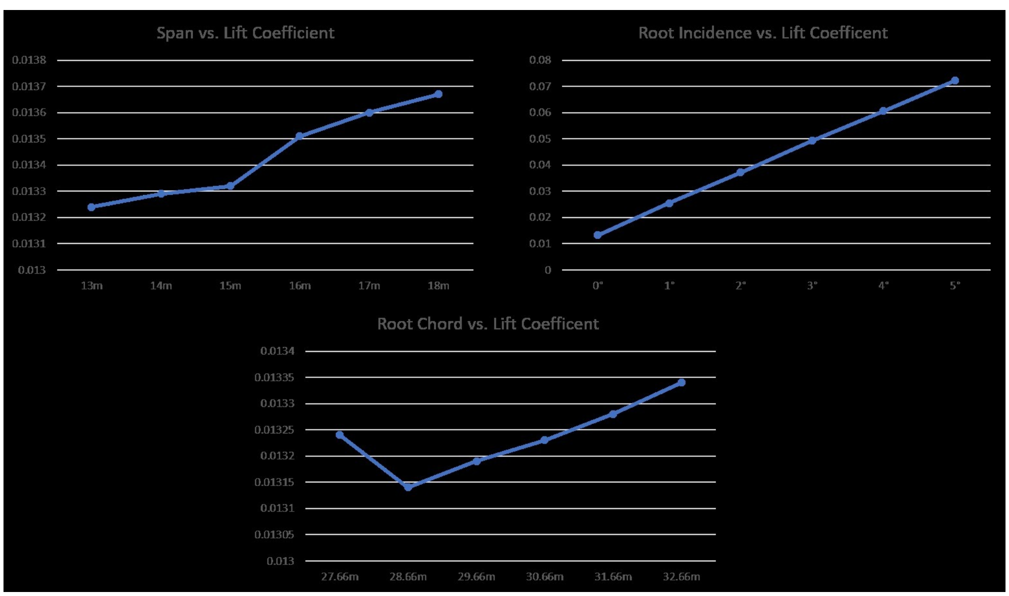

Figure 8: Relationship between span length, root incidence angle, and root chord length on the aerodynamic property of lift coefficient.

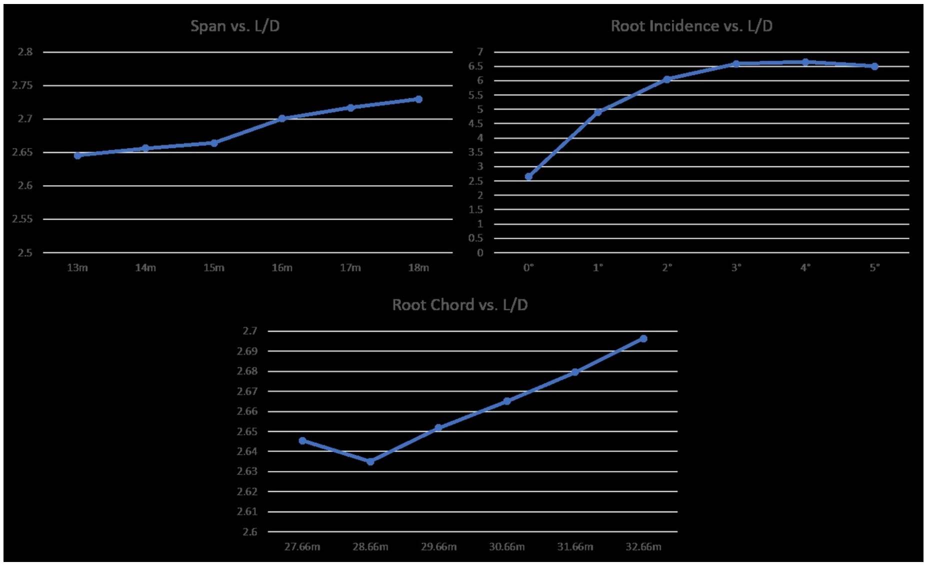

Figure 9: Relationship between span length, root incidence angle, and root chord length on the aerodynamic property of L/D.

Changing the span, and root chord (root incidence neglected) caused a negligible decrease in the skin friction drag coefficient. The largest non-significant change in skin friction coefficient was caused by increasing the root chord, where the skin friction coefficient gradually decreased from 0.00294 at the 27.66 m base to 0.00288 at 32.66 m. It is important to note that even though both parameters caused a decrease in the skin friction coefficient, the actual skin friction drag is increasing, because the wetted area and reference area both increase.

Changing the span and root chord caused a negligible increase in the lift coefficient (Figure 8), whereas increasing the root incidence caused the lift coefficient to significantly increase in a linear manner from 0.01324 at the 0° base to 0.07218 at 5°.

Increasing the span and root chord caused observable but negligible increases in the L/D (Figure 9). Increasing the root incidence greatly increased the L/D, which eventually approached a maximum. The largest change in L/D was caused by increasing the root incidence, where the L/D increased from 2.64549 at base 0° to 6.65488 at base 4°; and then gradually decreased to 6.4952 from 4° to 5°.

Analysis

The increase in span leading to the largest increase in the wave drag coefficient compared to the other parameters can be explained by assuming that the increase in span provides a better cross-sectional distribution across the aircraft.

The increase in root incidence leading to the largest increase in the induced drag coefficient compared to the other parameters is explained by analyzing the effect it has on the overall lift of the aircraft. Increasing the root incidence results in a higher coefficient of lift as per figure 7, and overall, resulting in a higher lift force. Induced drag is directly proportional to the overall lift force, so it can be assumed that a higher lift force would result in a higher induced drag coefficient.

The increase in root incidence also led to the largest increase in the lift coefficient compared to the other parameters. This is because increasing the root incidence leads the root aerofoil to have a higher angle facing the airflow. This in turn leads to a greater increase of pressure on the bottom surface of the aerofoil which means a higher pressure difference with the top of the aerofoil (20). This leads to more lift which in this study can be assumed to lead to a higher coefficient of lift.

The increase in root incidence also led to the largest increase in the L/D compared to the other parameters. This is because the coefficient of lift increased the lift coefficient the most compared to the other parameters while causing negligible differences in the increase of most of the drag coefficients with the other parameters according to figure 7. However, the induced drag coefficient increased the most with the increase in root incidence as well, which resulted in the total drag coefficient to steadily increase to a point where the L/D reached a maximum and started to steadily drop.

The increase in root chord leading to the largest increase in the skin friction drag coefficient compared to the other parameters can be explained by a greater increase in the wetted area than the increase in span. This evidently would lead to a higher skin friction drag coefficient.

Table 5 shows the values obtained from changing the span, Table 6 shows the results obtained from changing the root incidence, and Table 7 shows the results obtained from changing the root chord.

Table 5: Effect of changing the span on various design variables

Span	L/D	C_{D_f}	C_{D_w}	C_{D_i}	C_l
13m	2.64549	0.002937	0.0012	0.00061	0.01324
14m	2.65619	0.002935	0.0012	0.00061	0.01329
15m	2.66395	0.002934	0.0012	0.00061	0.01332
16m	2.70037	0.002932	0.0011	0.00061	0.01351
17m	2.71647	0.002931	0.0010	0.00061	0.01360
18m	2.72978	0.002930	0.0010	0.00061	0.01367

Table 6: Effect of changing the root incidence on various design variables

Root incidence	L/D	C_{D_f}	C_{D_w}	C_{D_i}	C_l
0°	2.64549	Negligible	0.0012	0.00061	0.01324
1°	4.89744	Negligible	0.0012	0.00082	0.02552
2°	6.04393	Negligible	0.0012	0.00175	0.03718
3°	6.58770	Negligible	0.0012	0.00306	0.04926
4°	6.65488	Negligible	0.0013	0.00467	0.06067
5°	6.49520	Negligible	0.0013	0.00663	0.07218

Table 7: Effect of changing the root chord on various design variables

Root Chord	L/D	C_{D_f}	C_{D_w}	C_{D_i}	C_l
27.66m	2.64549	0.002937	0.0012	0.00061	0.01324
28.66m	2.63496	0.002918	0.0012	0.00061	0.01314
29.66m	2.65181	0.002899	0.0012	0.00062	0.01319
30.66m	2.66511	0.002900	0.0012	0.00063	0.01323
31.66m	2.67949	0.002881	0.0012	0.00063	0.01328
32.66m	2.69637	0.002882	0.0011	0.00064	0.01334

Optimization

After identifying the relationship between the design parameters and their effect on this design study's variables, an equation was derived for each relationship. Ax (Adaptive Experimentation Platform), an optimization program that runs on python, was run to graph the equations on a multi-dimensional graph, and then evaluate the design parameters that yielded the best L/D within the bounds of each design iteration. The program's evaluation time was ~30 seconds.

Optimization equations

The relationship between span and L/D, that between root incidence and L/D and that between root chord and L/D were respectively best described by the equations:

$$z=0.0182\,x_1+2.6215,\{1\le x_1\le 6\}$$

$$z=-0.2924\,x_2^{\,2}+2.7631\,x_2+0.3184\,,\{1\le x_2\le 6\}$$

$$z=0.0115\,x_3+2.6221,\{1\le x_2\le 6\}$$

Where: $z=L/D$, x_1 = span length, x_2 = root incidence and x_3 = root chord length

The x-values from 1 to 6 correspond respectively to the increments of the x-axis of the plots in Figure 5, and Figure 6. (An x-value of 1 would correspond to a span length of 13 m, root incidence of 0°, and root chord length of 27.66 m).

Optimization process

An optimization program was run that combined each function to evaluate the best-estimated design parameter values by creating a multi-dimensional graph (Figure 10). These values created the aircraft with the best theoretical L/D within the bounds of each design iteration (Figure 11). Table 8 gives the values output by the optimization program.

Table 8: Optimization program output

Design Parameter	**Best Value**
x_1 (Span length)	x=6 (18m)
x_2 (Root incidence)	x=5 (5°)
x_3 (Root chord length)	x=6 (32.66m)

Specifications of the optimized aircraft

Table 9 provides the values for the main specifications of the wing, and theoretical L/D of the optimized 50-passenger aircraft for Mach 5 flight (Tip Chord is the length of the chord at the tip of the wing and Sweep is the angle the wing is swept back from its root).

Table 9: Final specifications

Wing Specifications and L/D	**Value**
Span	18m
Root Incidence	4°
Root Chord	32.66m
Tip Chord	5.6m
Sweep	73.5°
Aspect Ratio	0.87
Theoretical L/D	12.2658

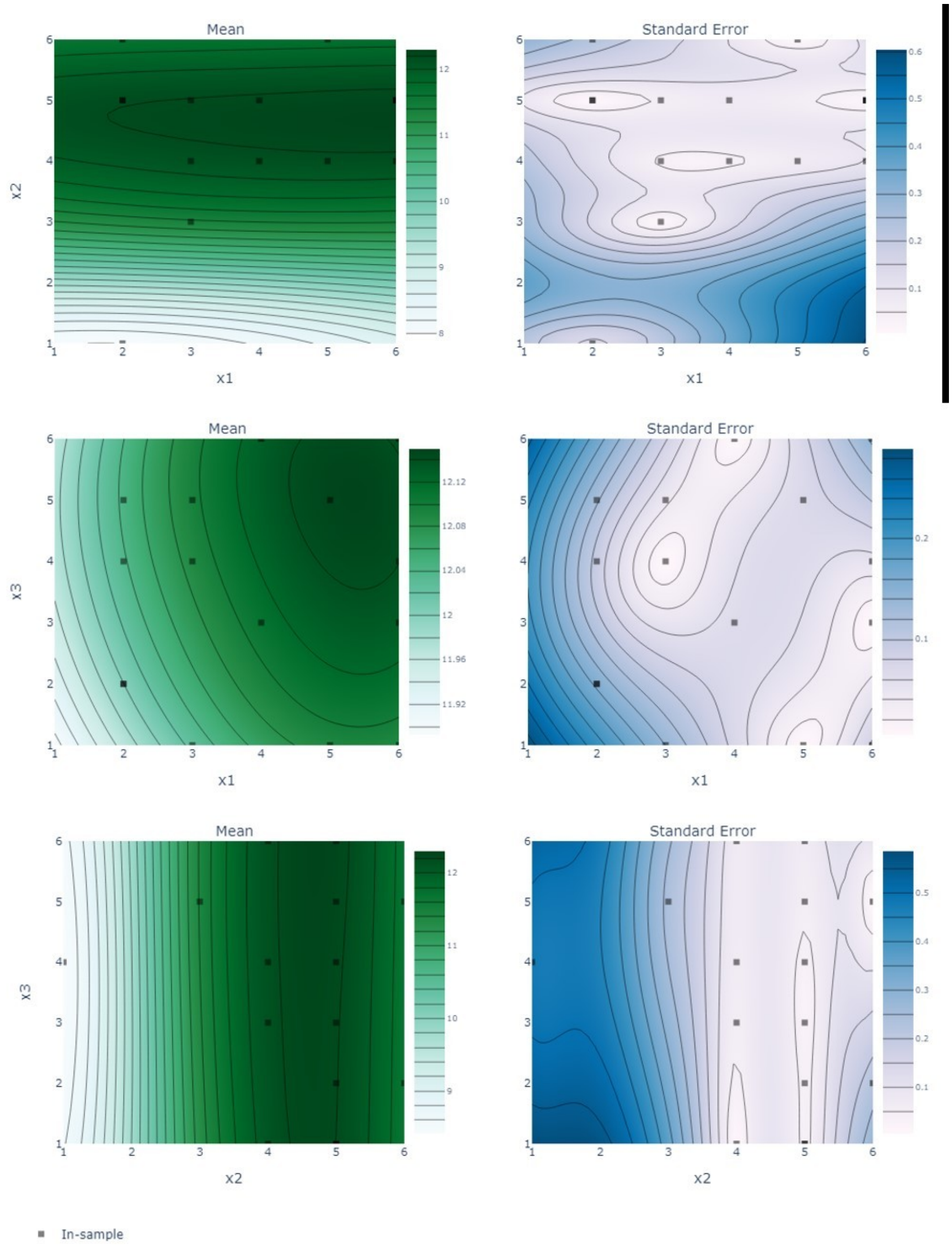

Figure 10: Each possible relation of each axis of the multi-dimensional graph graphed as two-dimensional contour graphs. The "In-samples" are points where the program was searching for the best parameter values.

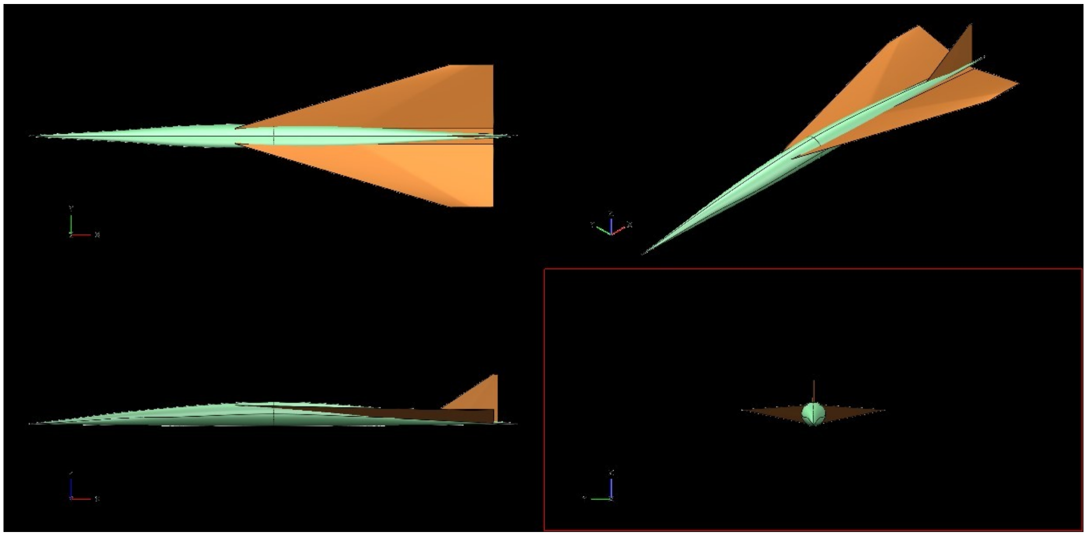

Figure 11: Final aircraft design in a top, side, front and isometric view that was optimized to achieve the best theoretical L/D.

Acknowledgments
I would like to thank my Polygence mentor Tanay Topak, a Ph.D. student of aerospace engineering, who supported me throughout the entire research and taught me valuable information of aerospace engineering, python programming, and optimization processes. I would also like to thank my Dad, as he was also always there to help in any way he could.

Nomenclature:

L/D**:** Lift-to-Drag Ratio – the ratio between coefficient of lift and coefficient of total drag; measures aerodynamic performance.

C_l**:** Coefficient of Lift – Dimensionless value that relates a lifting surface with the fluid around it.

C_D**:** Total Coefficient of Drag – Dimensionless value that relates the drag on a surface with the fluid around it.

D_f**:** Total Drag Force – The total force of drag (including all of its components) acting on a body.

C_{D_f}**:** Skin Friction Drag Coefficient – Dimensionless value that relates the skin friction drag on a surface with the fluid around it.

S_{ref}**:** Reference Area – The wing area from a top-down view.

ρ**:** Local Density of Air – The density of the air in the area the air is being measured.

V_∞**:** Free Stream Velocity – The velocity of the air relative to the lifting surface that is infinitely ahead of the lifting surface.

$\Re$**:** Reynolds Number – Dimensionless value that determines the state of the fluid flow (turbulent or laminar)

L**:** Characteristic Length – The volume of a body divided by its surface area.

μ**:** Flow Viscosity – The resistance to deformation of a fluid at a given rate ("thickness" of the fluid).

M**:** Mach Number – Value that determines how much a speed of a body is how many times over the speed of sound.

C_f**:** Flat Plate Average Laminar Coefficient of Friction, Flat Plate Average Turbulent Coefficient of Friction, Overall Laminar Coefficient of Friction (Depending on Situation) – Dimensionless value that relates the friction force on a surface with the fluid around it.

L_{ref}**:** Reference Length – The length of a body that is normal to a fluid flow.

$\bar{c}$**:** Weighted Chord Sum – The total average chord sum of a lifting surface.

S_{total}**:** Total Area – Total surface area of a body.

FF**:** Form Factor – Value that determines how "aerodynamic" a body is within a certain fluid flow.

t/c**:** Thickness-to-Chord Ratio – Ratio between the thickness of an aerofoil to its chord.

$\%Lam$**:** Percent of Laminar Flow – Percent of flow of a fluid that is laminar.

S_{wet}**:** Wetted Area – area of a body that is in contact with a fluid flow.

Q: Interference Factor – Factor used to calculate flat plate drag on an object.

References

1. S. A. Carioscia, J. W. Locke, I. D. Boyd, M. J. Lewis, and R. P. Hallion, "2. challenges to supersonic flight - jstor.org," *Commercial Development of Civilian Supersonic Aircraft*, 01-Aug-2019. [Online]. Available: https://www.jstor.org/stable/resrep22822.5

2. "Friction drag coefficient," *Friction Drag Coefficient - an overview | ScienceDirect Topics*. [Online]. Available: https://www.sciencedirect.com/topics/engineering/friction-drag-coefficient

3. “Friction drag,” *SKYbrary Aviation Safety*. [Online]. Available: https://skybrary.aero/articles/friction-drag#:~:text=Friction%20Drag%2C%20also%20known%20as,the%20square%20of%20the%20velocity

4. A. K. Dey, “What is the Reynolds number? the equation for Reynolds number and its significance (with PDF),” *What is Piping*, 25-Dec-2021. [Online]. Available: https://whatispiping.com/reynolds-number/#:~:text=Factors%20Affecting%20Reynolds%20Number,velocity%20the%20Reynolds%20number%20increases

5. “Hypersonic speed,” *Hypersonic Speed - an overview | ScienceDirect Topics*. [Online]. Available: https://www.sciencedirect.com/topics/engineering/hypersonic-speed

6. S. A. Carioscia, J. W. Locke, I. D. Boyd, M. J. Lewis, and R. P. Hallion, “2. challenges to supersonic flight - jstor.org,” *Commercial Development of Civilian Supersonic Aircraft*, 01-Aug-2019. [Online]. Available: https://www.jstor.org/stable/resrep22822.5

7. A. S. Thomas, W. S. Saric, A. L. Braslow, D. M. Bushnell, Poisson-Quinton, R. C. Lock, J. E. Hackett, and Advisory Group For Aerospace Research And Development Neuilly-Sur-Seine (France), “Aircraft drag prediction and reduction,” *DTIC*. [Online]. Available: https://apps.dtic.mil/sti/citations/ADA160718

8. R. T. Jones, “Theory of wing-body drag at supersonic speeds - NASA technical reports server (NTRS),” *NASA*, 06-Sep-2013. [Online]. Available: https://ntrs.nasa.gov/citations/19930092281

9. “Bow shock (aerodynamics),” *Academic Dictionaries and Encyclopedias*. [Online]. Available: https://en-academic.com/dic.nsf/enwiki/4873399

10. “Chapter 4,” *Compressible Flow*. [Online]. Available: https://compflow.onlineflowcalculator.com/Anderson/Chapter4/print/

11. S. Karadi, “Diamond-airfoil wing analysis,” *Medium*, 02-Oct-2021. [Online]. Available: https://medium.com/@shreyaskaradi2004/diamond-airfoil-wing-analysis-837874169583

12. S. Athul Krishna and M. R. Aswin, “Comparative study over double wedge and biconvex airfoils for laminar flow using CFD,” *Journal of Physics: Conference Series*, vol. 2272, no. 1, p. 012003, 2022.

13. S. P. R. Gopavaram and J. Sushma, “Aerodynamic investigation of double wedge supersonic airfoil,” *International Journal of Engineering Research & Technology*, 02-Jul-2019. [Online]. Available: https://www.ijert.org/aerodynamic-investigation-of-double-wedge-supersonic-airfoil

14. A. Filippone, “Aerodynamics of the delta wing,” *aerodyn*. [Online]. Available: https://aerodyn.org/delta/

15. “Sears-Haack body,” *Swyde*, 05-Jan-2015. [Online]. Available: https://swyde.com/s/Sears-Haack_body

16. “OpenVSP,” *start [OpenVSP]*. [Online]. Available: http://openvsp.org/wiki/doku.php

17. “OpenVSP,” *vspaerotutorial [OpenVSP]*. [Online]. Available: http://openvsp.org/wiki/doku.php?id=vspaerotutorial&s%5B%5D=vspaero

18. “OpenVSP,” *parasitedrag [OpenVSP]*. [Online]. Available: http://openvsp.org/wiki/doku.php?id=parasitedrag#general_overview

19. “OpenVSP,” *wavedrag [OpenVSP]*. [Online]. Available: http://openvsp.org/wiki/doku.php?id=wavedrag

20. “How an airfoil's angle of attack creates lift and drag,” Cadence, 13-Dec-2022. [Online]. Available: https://resources.system-analysis.cadence.com/blog/msa2022-how-an-airfoils-angle-of-attack-creates-lift-and-drag